WILEY-VCH

A Tunable Soft Silicone Bioadhesive for Secure Anchoring of Diverse Medical Devices to Wet Biological Tissue

*Manisha Singh[1], Debbie L. Teodorescu[2], Meagan Rowlett[3], Sophie X. Wang[1,4], Mercedes Balcells[1,5], Clara Park[1,6], Bruno Bernardo[1], Sian McGarel[1], Charlotte Reeves[1], Mandeep R. Mehra[7], Xuanhe Zhao[6], Hyunwoo Yuk[6,8], Ellen T. Roche[1,6]**

[1]Institute for Medical Engineering and Science, Massachusetts Institute of Technology, Cambridge, MA, USA.

[2]Department of Cardiology, Cedars-Sinai Smidt Heart Institute, Los Angeles, CA, USA.

[3]Department of Biological Engineering, Massachusetts Institute of Technology, Cambridge, MA, USA.

[4]Department of Surgery, Beth Israel Deaconess Medical Center, Boston, MA, USA.

[5]Bioengineering Department, Institut Químic de Sarrià, Ramon Llull Univ, Barcelona, Spain

[6]Department of Mechanical Engineering, Massachusetts Institute of Technology; Cambridge, MA, USA.

[7]Brigham and Women's Hospital and Harvard Medical School, Boston, MA, USA.

[8]SanaHeal, Inc., Cambridge, MA, USA.

**Corresponding author:

Ellen T. Roche. Email: etr@mit.edu

Abstract

Silicone is utilized widely in medical devices for its compatibility with tissues and bodily fluids, making it a versatile material for implants and wearables. To effectively bond silicone devices to biological tissues, a reliable adhesive is required to create a strong and long-lasting interface. This study introduces BioAdheSil, a silicone-based bioadhesive designed to provide robust adhesion on both sides of the interface, facilitating bonding between dissimilar substrates, namely silicone devices and tissues. The adhesive's design focuses on two key aspects: wet tissue adhesion capability and tissue-infiltration-based long-term integration. BioAdheSil is formulated by mixing soft silicone oligomers with siloxane coupling agents and absorbents for bonding the hydrophobic silicone device to hydrophilic biological tissues. Incorporation of biodegradable absorbents eliminates surface water and controls porosity, while silane crosslinkers provide interfacial strength. Over time, BioAdheSil transitions from non-permeable to permeable through enzyme degradation, creating a porous structure that facilitates cell migration and tissue integration, potentially enabling long-lasting adhesion. Experimental results demonstrate that BioAdheSil outperforms commercial adhesives and elicits no adverse response in rats. BioAdheSil offers practical utility for adhering silicone devices to wet tissues, including long-term implants and transcutaneous devices. In this study, we demonstrate its functionality through applications such as tracheal stents and LVAD (Left Ventricular Assist Device) lines.

Keywords: wet tissue adhesive; silicone devices; tissue integration; long term adhesion

Introduction

Silicones are increasingly used in medicine and healthcare applications due to their desirable properties, including chemical stability, mechanical strength, constant performance across varying physical conditions, and compatibility with living tissues.[1-5] Used in both internal and external medical devices, applications include implants, prosthetics, intravenous drug and transfusion delivery systems, stents, breathing tubes, and catheters.[1-2, 4] The market for silicone in medical applications is projected to reach 656.5 million USD by 2025, with a volume consumption of 47.7 kilotonnes.[2, 4] Owing to its chemical inertness, silicone is a widely used biocompatible material, but it also is challenging to adhere to substrates like biological tissues that are dissimilar and wet. As a result, implantable silicone devices like tracheal stents, pacemaker leads, cerebrospinal fluid shunts, and peritoneal dialysis lines are often left untethered, making them prone to migration from the intended site.[6] Alternatively, they may be anchored using mechanical techniques such as hooks, sutures, and screws, but this causes trauma and tissue erosion due to mechanical mismatch.[7-9] For example, a percutaneous endoscopic gastrostomy (PEG) tube is often secured in place using mechanical bumpers that compress the abdominal wall. Over time, excessive compression causes changes in the tissue's mechanical properties and leads to dislodgment of the PEG tube, resulting in buried bumper syndrome.[10] For challenging applications, such as ostomies, stomas, left ventricular assist device (LVAD) drivelines, and peritoneal catheters, new strategies for long-term fixation are necessary, as existing dressings, tapes, and bandages result in leakage of biofluids as well as the formation and migration of biofilms over time.[11-12]

Manufacturers of adhesives encounter various design challenges when attempting to securely attach silicone devices to living tissues. The desired adhesive must provide robust and reliable adhesion not only to the underlying biological tissues but also to the silicone medical device. Moreover, this adhesive must incorporate specific design features to overcome surface water challenges when bonding implantable devices to moist tissues. Additionally, for the long-term fixation of transcutaneous catheters and implantable heart devices with drivelines, the adhesive design should offer consistent and impenetrable resistance against biofluids to prevent biofilm migration.

While existing hydrophilic adhesives initially offer strong adhesion, they tend to weaken over time due to factors like exposure to moisture, swelling, and the complete degradation of adhesive materials. A hydrophobic, partially degradable adhesive material could provide a comprehensive long-term solution for implant fixation by incorporating the following features. The hydrophobic nature would offer resistance to moisture and degradation, ensuring enduring adhesion strength, especially crucial for long-term implant fixation. Partial degradability of the adhesive would allow for gradual breakdown over time, releasing biocompatible byproducts that can be readily absorbed or metabolized by the surrounding tissue. Consequently, the partially degradable component could create pathways or spaces within the adhesive matrix, facilitating cell migration and promoting seamless integration of the device with the host tissue. Such an adhesive would encourage tissue integration around the implant, thereby providing lasting adhesion.

Equipped with the aforementioned design features, we introduce BioAdheSil, a silicone-based bioadhesive designed for effective bonding of silicone devices to wet tissues. BioAdheSil is formulated with siloxane coupling agents, silane crosslinkers, and biodegradable absorbents (e.g., starch, carbopol). Silane crosslinkers facilitate the bonding at the interface and can be adjusted to

fine-tune the adhesion strength. Absorbent additives eliminate surface water upon contact and produce a matrix whose porosity can be controlled by altering their weight. Experiments have been carried out to investigate the impact of crosslinkers and additives on adhesion, taking into account their concentration and the type of substrate. Our findings demonstrate that BioAdheSil yields stronger adhesion between tissues and silicone devices compared to commercially available adhesives. This work establishes a framework for a rapid-curing, tunable, non-porous adhesive interface, which can be programmed to become porous naturally via enzymatic degradation, resulting in long-lasting adhesion by enabling cell migration. Examples of silicone medical devices adhered using BioAdheSil, such as long-term synthetic implants and transcutaneous devices, showcase the versatility, broad applicability, and practicality of the materials and concepts discussed in this study.

Results and Discussion

Adhesive Formulation and Mechanism

A wide range of healthcare applications can benefit from adhesive bonding between dissimilar biological tissues and silicone medical devices (**Figure 1a**). Our approach to developing a silicone-to-tissue adhesive, called BioAdheSil, involves a platinum-catalyzed silicone precursor (polydimethylsiloxane, PDMS, or Ecoflex) and a siloxane coupling agent. A silicone precursor is chosen for its ability to integrate with the silicones found on medical device surfaces.[13] The siloxane coupling agent is copolymerized with the silane crosslinker (i.e., triethoxy vinyl silane, TEVS) into a silicone polymer network. This creates silanol groups (Si-OH) in the presence of water (**Figure 1b**, Supplementary **Figure S1**). Simultaneously, the silane crosslinker (i.e., triethoxy(3-isocyanatopropyl)silane, TEPI) in the adhesive matrix forms covalent bonds with the tissue surface, creating triethoxysilane groups on the tissue side (Supplementary **Figure S1**). The silane groups then hydrolyze into silanol in a hydrated environment. Next, the silanol groups from tissue and silicone combine to condense and form a siloxane bond, resulting in water as a by-product (**Figure 1b**). The excess interfacial water is absorbed by biodegradable and water-absorbent additives like starch or carbopol, thereby creating water free crosslinking surfaces. The resulting chemical design facilitates strong bonding at the interface on both sides, meeting the requirements for a variety of implantable silicone devices. The proposed interfacial adhesion mechanism involving the condensation of silanol (Si-OH) groups into siloxane (Si-O-Si) is confirmed by ATR-FTIR (Attenuated Total Reflectance Fourier-Transform Infrared Spectroscopy) in **Figure 2a**. BioAdheSil was cured in real-time on a tissue substrate, and FTIR spectra were recorded from t0 to t7 over a duration of 15 min. **Supplementary Figure S2** displays the separate FTIR spectra of the tissue specimen and the cured adhesive. The FTIR spectra in **Figure 2a** provide the following wavenumber peak assignments: 3374 cm^{-1}: corresponding to the stretching vibration of associated O-H. Its intensity decreased with curing time (from t0 to t7), indicating a reduction in -OH groups during curing (**Figure 2b**); 1010 cm^{-1}: representing the stretching vibration of Si-O. Its intensity increased with curing time, suggesting the formation of siloxane-based covalent crosslinking at the interface (**Supplementary Figure S3**); 787 cm^{-1}: Signifying the bending vibrations of Si-O. Its intensity also increased with curing time (**Figure 2c**). Additional bands at 1646 cm^{-1} and 1258 cm^{-1} correspond to the stretching of C=C and symmetric deformation vibrations of Si-C, respectively.

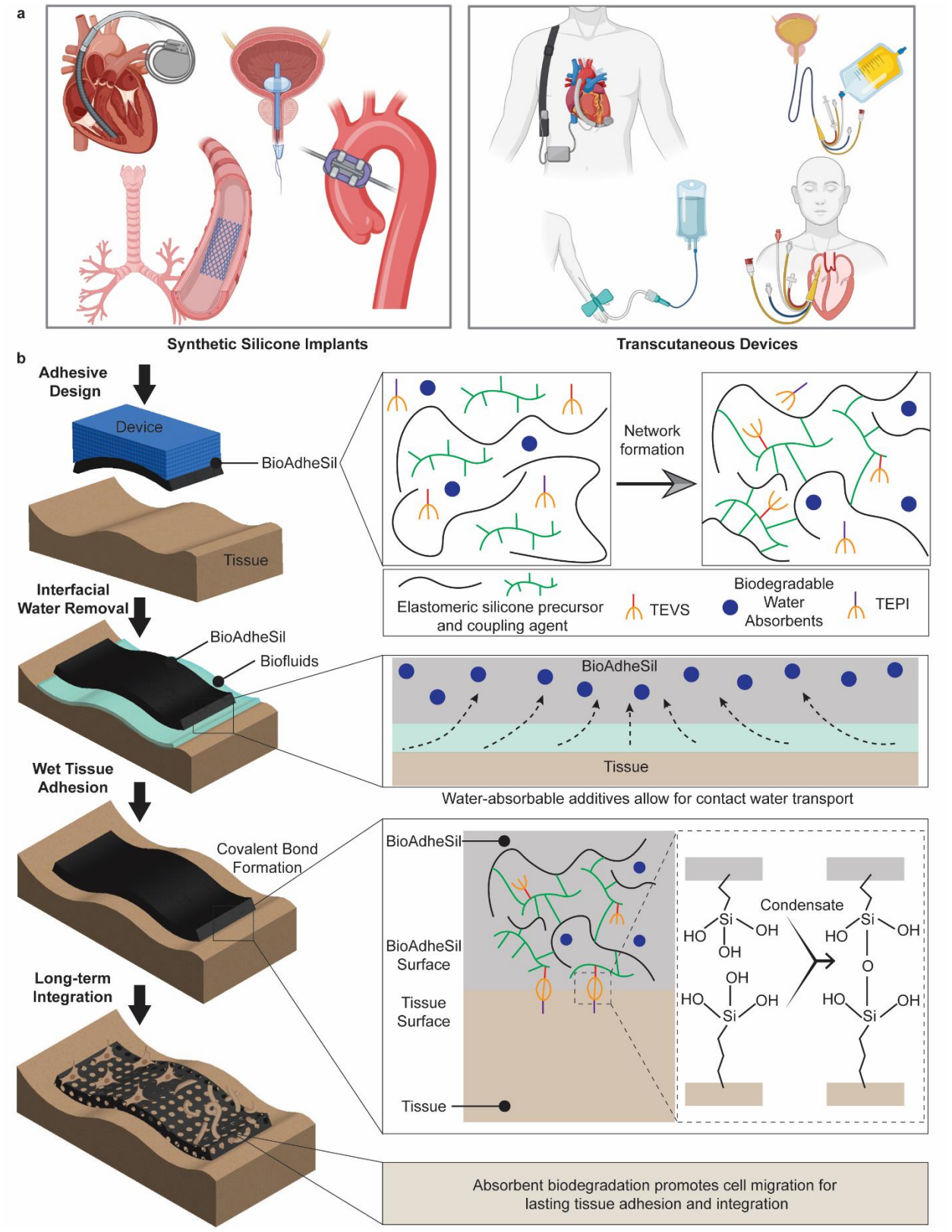

Figure 1: Overview and adhesive mechanism. (a) Schematic illustrations demonstrate examples of diverse silicone medical devices that can be adhered to wet biological tissues using BioAdheSil, a silicone-based bioadhesive. (b) Crosslinking mechanism and adhesive chemistry of

BioAdheSil for bonding silicone devices to biological tissues. TEVS, triethoxy vinyl silane; TEPI, triethoxy(3-isocyanatopropyl)silane.

Adhesive Characterization for Optimal Design and Performance

The concentration of silane crosslinkers (TEVS and TEPI) plays a crucial role in determining the interfacial strength of the BioAdheSil technology. We assess the interfacial crosslinking by varying the concentration from 0.5 to 1.5% in a silicone matrix and testing against hydrated tissue mimics, specifically collagen sheets, using the lap-shear method. BioAdheSil reaches a maximum crosslinking strength of 143 ± 9 kPa at a concentration of 1.5% (**Figure 2d**). Increasing the concentration beyond 1.5% leads to notably longer curing times.

To investigate the influence of different TEVS and TEPI ratios on the interfacial crosslinking of BioAdheSil, we systematically varied the TEVS: TEPI ratio across a range, including 1:1, 1:0, 0:1, 1:2, and 2:1 (**Supplementary Figure S4**). Our findings reveal that adjusting these ratios allows for precise fine-tuning of the adhesive properties. The highest interfacial strength was achieved with a TEVS to TEPI ratio of 1:2. A higher TEPI ratio relative to TEVS was observed to enhance crosslinking sites on tissues, resulting in increased adhesive strength. Conversely, a higher TEVS ratio led to a reduction in interfacial strength, likely due to the condensation of silanol (Si-OH) groups within the bulk adhesive matrix. Importantly, the absence of either TEVS or TEPI reduced interfacial adhesion.

The crosslinked BioAdheSil exhibits mechanical properties that are comparable to those of soft tissues.[14-15] BioAdheSil demonstrates a tensile strength range of 600-1000 kPa and can elongate up to 900% (**Figure 2e**).

The removal of surface water is critical to avoid adhesion fouling at the interface. To address this, we explored the absorption of interfacial water through absorbents such as starch and carbopol. The lap-shear test performed on wet collagen sheets determined the optimal amounts of water-absorbent additives (**Figure**s **2f, 2g**). We experimented with weight percentages ranging from 0 to 30% for carbopol and up to 60% for starch. Our findings indicate that the optimal adhesion strengths of approximately, 97 ± 13, and 162 ± 8 kPa are achieved at 5 wt% for carbopol, and 30 wt% for starch, respectively. The maximum interfacial adhesion strength for carbopol and starch-based formulations are 62% and 170% higher, respectively, than the control formulation with no additives

Other water-absorbing agents can be employed as additives for BioAdheSil. In this study, alongside starch and carbopol, we have also investigated the influence of calcium sulfate, a widely used desiccant. Calcium sulfate was tested at 5 wt%, 15 wt%, and 30 wt% to assess its impact on the shear adhesion strength of our silicone-based adhesive and provides comparable adhesion strength to starch and carbopol-based formulations (**Supplementary Figure S5**).

To study swelling behavior, cured samples of known weights were completely submersed in phosphate-buffered saline (PBS) and their weights were monitored over an extended period, with weight measurements taken at regular intervals from Day 0 to Day 5. The results are shown in the **Supplementary Figure S6**. The adhesive's volumetric shrinkage during the curing process was determined to be 8.76 ± 2.42% through measurements taken while curing the adhesive in a known-sized mold (**Supplementary Figure S7**).

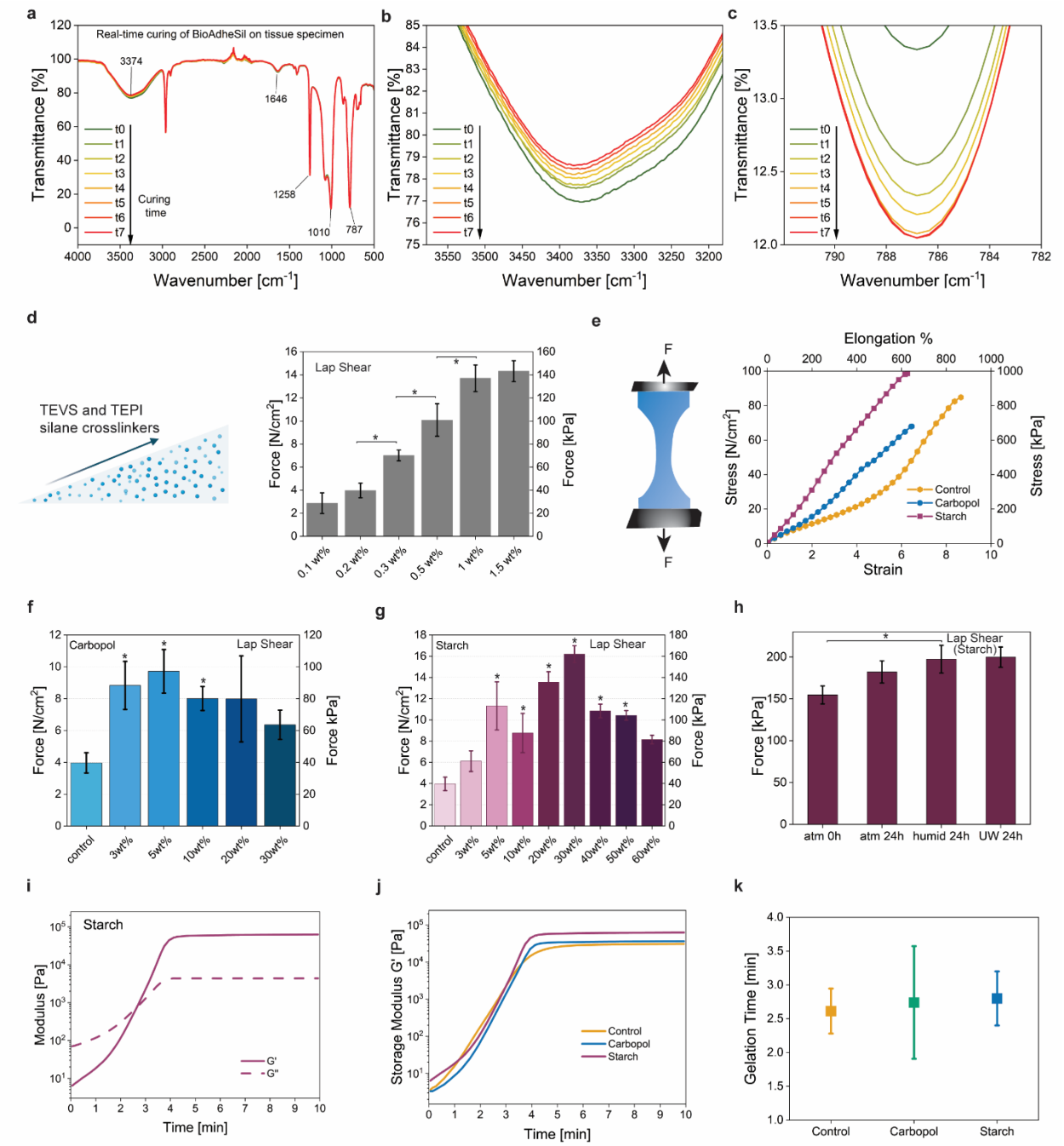

Figure 2: Adhesion mechanism, design, and characterization for optimal crosslinking. (a) Monitoring the real-time curing of BioAdheSil on tissue substrate with ATR FTIR (Attenuated Total Reflectance Fourier-Transform Infrared spectroscopy). (b) ATR FTIR evaluation of adhesion mechanism showing a reduction in OH band intensity during real-time curing, indicating the removal of silanol groups. (c) ATR FTIR evaluation of adhesion mechanism demonstrating an increase in Si-O band intensity at 787 cm^{-1} during real-time curing, signifying siloxane bond formation. (d) Impact of TEVS and TEPI crosslinkers on the adhesion; tested using the lap-shear method against silicone and tissue-mimic collagen sheets. TEVS, triethoxy vinyl silane; TEPI, triethoxy(3-isocyanatopropyl)silane. (e) Uniaxial tensile testing of cured BioAdheSil with 30 wt% starch, 5 wt% carbopol, and no additives as control. (f) Effect of water-

absorbent carbopol on interfacial adhesion against hydrated collagen sheets using a lap-shear test, with no additives as control. The statistical analysis shown with * is performed against the control, $p<0.05$. (g) The impact of water-absorbent starch on interfacial adhesion against hydrated collagen sheets using the lap-shear test, with no additives as control. The statistical analysis shown with * is performed against the control, $p<0.05$. (h) Shear adhesion strength tests of water-absorbing additives pre- and post-24-hour exposure to humid environments with varying hydration levels. Atm, cured under atmospheric conditions; UW, cured underwater. (i) Real-time rheology of BioAdheSil with 30 wt% starch. G' storage modulus, G" loss modulus. (j) Comparison of storage modulus (G') between 30 wt% starch, 5 wt% carbopol, and control (no additives). (k) Gelation time ($G' = G''$) for BioAdheSil with 30 wt% starch, 5 wt% carbopol, and control, no additives used. Values represent the mean and standard deviation (n=3), $*p<0.05$.

To study the behavior of water-absorbing additives under humid conditions, we conducted shear adhesion strength tests before and after exposing the samples to a 24-hour humid environment with varying hydration levels, including moisture and complete submersion. Surprisingly, interfacial adhesion increased with higher hydration levels over time (**Figure 2h**). This increase can be attributed to water-absorbent additives in the adhesive, enhancing interfacial strength by exposing additional hydroxyl groups. These hydroxyl groups can potentially react to form more siloxane bonds, depending on the rate of silane hydrolysis and condensation.

BioAdheSil, prior to curing, is a viscous polymer material that can be applied to tissue and device surfaces in a conformal manner through custom-designed applicators or catheter injection. Real-time rheological studies verify its viscous properties, as shown in **Figure 2i**. The storage modulus (G') is lower than the loss modulus (G") prior to curing, but the opposite occurs as crosslinking begins, indicating a change from a viscous liquid to an elastomeric solid. The crosslinked matrix attains full strength within 10 minutes, with a gelation time of less than three minutes, as demonstrated in **Figure**s **2j** and **2k**. The addition of water absorbents or repellents does not significantly impact the storage modulus or gelation time of the adhesive.

After determining the optimal concentration of crosslinkers and additives, we assess the adhesion strength of BioAdheSil against wet porcine skin using two distinct mechanical testing methods. The T-peel test, in accordance with ASTM F2256-05, measures the interfacial toughness under tension loading, while the lap-shear method, following ASTM F2255-05, measures the interfacial shear strength under tension loading (**Figure 3a**). BioAdheSil provides an interfacial adhesion energy range of 800 to 1150 J m^{-2} and a shear adhesion strength of 70-100 kPa between silicone and hydrated porcine skin, as shown in **Figure**s **3b** and **3c**.

To assess long-term adhesion strength, we employed BioAdheSil to bond silicone and ex-vivo porcine skin samples, submerging them in phosphate-buffered saline (PBS) for up to 48 hours. Adhesive strength was measured at intervals of 0 hours, 24 hours, and 48 hours. The results consistently demonstrate that BioAdheSil maintains and even increases adhesion in hydrated conditions over time (**Supplementary Figure S8**). This behavior can be attributed to silane crosslinkers interacting with the hydrated surface. Alkoxy groups within the crosslinkers react with water, forming silanol groups (Si-OH), which then condense to create siloxane bonds (Si-O-Si). The greater the number of siloxane bonds formed, the stronger the connection between the silane and the surface. Furthermore, water absorption by water-absorbent additives in the

adhesive may enhance this process by exposing more hydroxyl groups on the substrate. These hydroxyl groups can subsequently react with the silane to generate siloxane bonds, contingent on the rate of hydrolysis and condensation of the silane. Of note, BioAdheSil does not provide repeated adhesion to a surface without a decline in its adhesive properties.

BioAdheSil has superior adhesion to silicone compared to commercial adhesives

The effectiveness of BioAdheSil and several commercially available tissue adhesives was evaluated for their bonding capability with both chemically stable materials, such as cellulose, and chemically inert materials, like silicone. Cellulose acetate, a modified plastic form of a natural material, was selected as the test substrate due to its ability to provide surface functional groups that are compatible with a wide array of commercially available tissue adhesives, as well as for BioAdheSil. The evaluation was conducted using lap-shear, 90-degree peel, and tack adhesion tests, as depicted in **Figure 3d**. A selection of various crosslinking mechanisms was employed for the commercial adhesives, including cyanoacrylate-based (Dermabond), polyethylene glycol-based (DuraSeal), albumin-based (BioGlue), and fibrin-based (Tisseel) chemistries. BioAdheSil demonstrated better bonding performance compared to Dermabond, DuraSeal, BioGlue, and Tisseel adhesives when applied to chemically stable cellulose substrates in all test methods except lap-shear testing (**Figure**s **3e**, **3f**, and **3g)**. BioAdheSil offers comparable shear strength to Dermabond and BioGlue. When tested on chemically inert materials like silicone, BioAdheSil showed significantly stronger adhesion strength compared to Dermabond and BioGlue, whose adhesion strength was reduced to half or less. BioAdheSil demonstrated four times higher shear strength, three times higher tack strength, and seven times higher peel force compared to Dermabond when tested on silicone substrates. This superiority is evident in **Figure**s **3e**, **3f**, and **3g**. In summary, BioAdheSil is more effective in bonding to chemically inert silicone materials compared to commercially available tissue adhesives. Its distinctive design and advantageous properties are compared to state-of-the-art adhesives (**Supplementary Table S1**).[16-21]

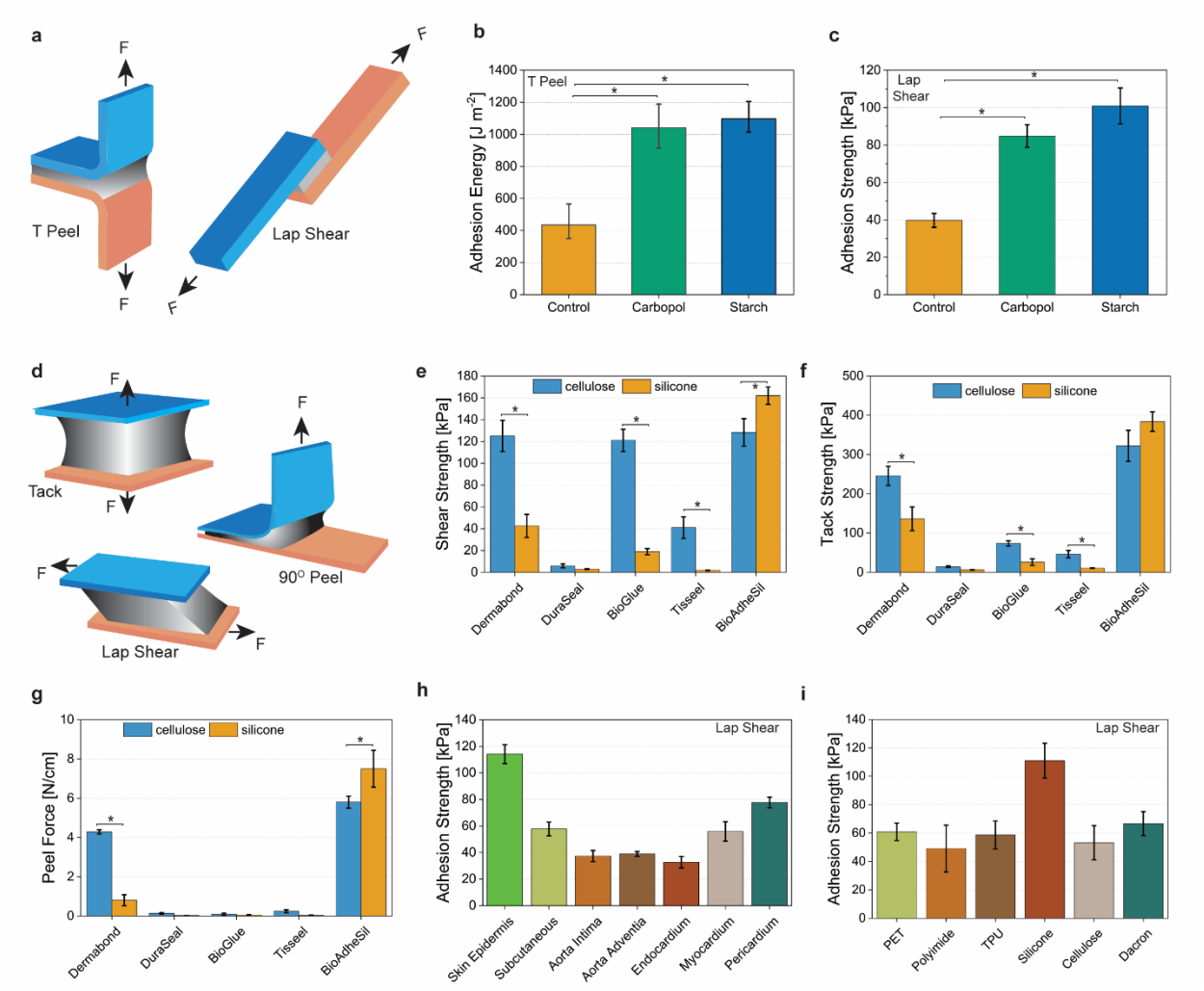

Figure 3: Benchmarking against commercial adhesives and adhesion strength of BioAdheSil against different substrates. (a) Schematics showing the T-peel and lap-shear testing setups. (b) Adhesion energy or interfacial toughness was measured between silicone and hydrated porcine skin via the T-peel method with 30 wt% starch, 5 wt% carbopol, and control (no additive). (c) Shear adhesion strength was evaluated between silicone and hydrated porcine skin using the lap-shear method with 30 wt% starch, 5 wt% carbopol, and control (no additive). (d)Test setup for tack, 90-degree peel, and lap-shear adhesion testing. (e) The shear adhesion strength of BioAdheSil compared with various commercial adhesives. (f) The tack adhesion of BioAdheSil compared with various commercial adhesives. (g) The peel force of BioAdheSil compared with various commercial adhesives. The shear, tack, and peel tests were performed against hydrated collagen sheets using silicone and cellulose as chemically inert and chemically stable synthetic substrates. (h) The shear adhesion strength of various biological tissues adhered to silicone substrates using BioAdheSil. (i) The shear adhesion strength of various synthetic engineering substrates adhered to hydrated porcine skin using BioAdheSil. PET, polyethylene terephthalate; TPU, thermoplastic polyurethane. Values represent the mean and standard deviation (n=3), *$p<0.05$.

A platform for adhering diverse materials to various substrates

The advantageous combination of high interfacial toughness, strong shear bonding, and rapid curing in BioAdheSil-with-starch renders it suitable for a wide variety of tissues and synthetic device materials. BioAdheSil adhesion is tested on a range of biological materials, such as the epidermis, subcutaneous tissue, intima, adventitia, endocardium, myocardium, and pericardium, as well as a diverse array of engineering substrates, including polyethylene terephthalate (PET), polyimide, thermoplastic polyurethane (TPU), silicone, cellulose, and Dacron polyester (as depicted in **Figure**s **3h** and **3i**). The shear adhesion strength between silicone and wet tissue surfaces is 114 ± 7 kPa for epidermal skin, 58 ± 5 kPa for subcutaneous skin tissue, 37 ± 4 kPa for inner layer of aorta, 40 ± 2 kPa for outer layer of aorta, 33 ± 4 kPa for inner lining of heart, 56 ± 7 kPa for heart muscle, and 78 ± 4 kPa for pericardium, the sac surrounding the heart. The shear adhesion strength of synthetic materials used as substrates or outer enclosures for medical devices is 61 ± 6 kPa for PET, 49 ± 16 kPa for polyimide, 59 ± 9 kPa for TPU, 111 ± 12 kPa for silicone, 53 ± 12 kPa for cellulose, and 67 ± 8 kPa for Dacron against wet porcine skin.

Our fabrication method is versatile and can be applied to different polymer networks as silane crosslinkers with different types of organofunctional groups are commercially available. This implies that the adhesion of BioAdheSil to the listed engineering substrates can be further improved by functionalizing their surfaces with various groups to achieve covalent bonding at the interface. Similarly, BioAdheSil could also be applied to challenging tissue substrates, such as the inner mucosal layer of intestinal tissues. One example we explored is using a combination of (3-Aminopropyl)triethoxysilane (APTES) and transglutaminase in place of the TEPI silane crosslinker in our TissuSil system. APTES has previously been shown to functionalize surface silanol groups with primary amines. [22-23] Transglutaminase was selected for its ability to catalyze the creation of a covalent bond between the free amine groups and the γ-carboxamide group or glutamine amino acids in tissues.[24] BioAdheSil with the transglutaminase pathway demonstrates a higher shear adhesion strength than BioAdheSil with siloxane for bonding to intestinal tissues (as seen in Supplementary **Figure S9**). The high viscosity and bonding properties of BioAdheSil could make it ideal for applications like closing gastrointestinal fistulas due to its ability to adhere to the intestinal lining. This chemistry-adjustable platform enables capabilities that have not been previously reported and opens new opportunities by broadening the range of materials and applications that can be utilized with our adhesive system.

Moreover, BioAdheSil can be made conductive by adding substances such as graphene ink composite, carbon nanotubes, or poly(3,4-ethylenedioxythiophene) polystyrene sulfonate and polyaniline polymers, allowing it to form functional interfaces.[25-28] For instance, incorporating multi-walled carbon nanotubes (CNTs) into BioAdheSil through physical mixing results in a conductive matrix with tunable resistance that ranges from 1.5 to 450 kilo-ohms by adjusting the amount of CNTs from 5 to 10 wt% (as seen in Supplementary **Figure S10**). This expands the possible uses of BioAdheSil to act as a flexible electronic skin that can seamlessly integrate with tissues as bioelectronic interfaces or electrodes, potentially allowing for both recording and stimulation capabilities.[29-30]

***In vivo* Biocompatibility Testing of BioAdheSil**

Pre-cured patches of BioAdheSil, (with 30% starch and without starch), were subcutaneously implanted in the dorsal region of a rat model (n=8 replicates from two rats) for a duration of 4 weeks to investigate the *in vivo* biocompatibility of the adhesive material (**Figure 4a**). For histological analysis, we implanted pre-cured adhesive. While using the precursor form, there were challenges associated with sterilizing the uncured liquid, that warrant further work. Histological evaluation conducted by a blinded pathologist revealed that neither the starch-based nor the non-starch-based samples elicit adverse or inflammatory reactions after the 4-week implantation period (**Figure 4b**). At 4 weeks, both implant types exhibit the formation of a fibrous capsule, with the thickness of the capsule slightly higher, though not significantly, in the non-starch case compared to the 30% starch-based BioAdheSil (**Figures 4c** and **4d**). No evidence of granulation tissue formation, necrosis of underlying dermal or muscular layers, or eosinophilic response indicative of allergic reactions was observed.

Furthermore, we assess the *in vivo* biocompatibility of BioAdheSil by conducting immunohistochemical analysis to evaluate the inflammatory foreign response using anti-CD68 antibodies. The immunohistochemical (IHC) staining of the biomarker, CD68, expressed by pro-inflammatory cells (macrophages and monocytes), is depicted in **Figure 4e**. Rabbit recombinant multiclonal anti-CD68 antibodies were used for IHC staining. To serve as negative controls, healthy tissues were extracted from the same rats from a region ~ 4 cm away from the site where BioAdheSil was implanted. Across three groups, healthy tissue (**Figure 4f)**, non-starch BioAdheSil (**Figure 4g)**, and 30% starch-based BioAdheSil (**Figure 4h)**, the IHC staining is indistinguishable in the bulk of the tissue, with a consistent concentration of total cells displaying positive staining for inflammatory cells in all three groups. Notably, at the interface between the implant and the surrounding tissue, as well as within the implant itself, an absence of CD68 cells is observed.

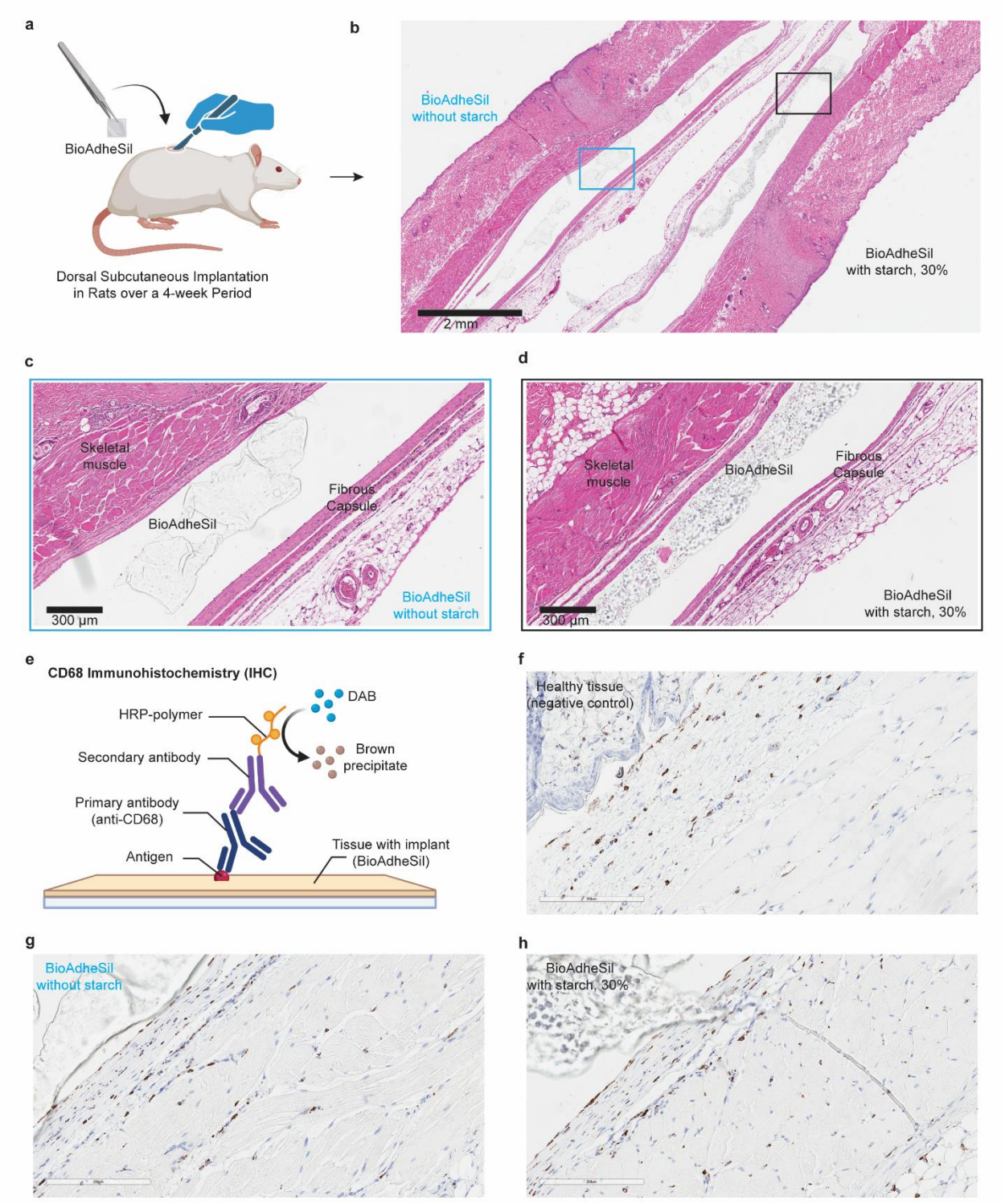

Figure 4: *In vivo* Biocompatibility of BioAdheSil. (a) A schematic illustration depicting the dorsal subcutaneous implantation of BioAdheSil, both with and without starch, in a rat model, for testing the *in vivo* biocompatibility. (b) Representative histological images of BioAdheSil, stained with hematoxylin and eosin (H&E), for both non-starch and 30% starch cases on the same slide after 4 weeks. (c) Representative histological images of subcutaneously implanted non-starch-based BioAdheSil stained with H&E after a 4-week duration (d) Representative histological

images of subcutaneously implanted 30% starch-based BioAdheSil stained with H&E after a 4-week period. (e) CD68 immunohistochemistry (IHC) analysis of immune response following 4-week implantation of BioAdheSil in the dorsal subcutaneous region. (f) IHC analysis of healthy tissue for CD68. (g) IHC analysis of tissues surrounding non-starch BioAdheSil for CD68. (h) IHC analysis of tissues surrounding 30% starch-based BioAdheSil for CD68. HRP, Horseradish Peroxidase; DAB, 3,3'-Diaminobenzidine.

Preventing migration of implantable airway stents

Airway stents are medical devices that are used to hold open and maintain the patency of the airway in patients with conditions such as tracheal stenosis, bronchial stenosis, airway fistulas, or lung cancer (**Figure 5a**).[31-32] They are typically made of medical-grade silicone and provide support to the airway wall and help prevent collapse or narrowing. Despite their therapeutic benefits, airway stent migration remains a significant concern. Stent migration is the unintended dislocation of the device from its initial placement within the airway, leading to complications like respiratory distress, recurrent symptoms, and the need for repeat interventions. This issue affects 5-20% of patients and may result from factors like stent sizing, design, or changes in airway anatomy due to disease progression.[32-33] Treatment depends on severity; partial migration may be managed conservatively with monitoring and potential stent repositioning via bronchoscopy. Severe cases with complete migration or airway obstruction require emergency intervention, which can include stent removal, replacement, or other procedures. Tethering airway stents with mechanical tools such as hooks or screws increases the risk of re-stenosis through fibrosis, as it can lead to the formation of granuloma.[32] Securing the stent in place using a biocompatible adhesive could provide an alternative solution and reduce the risk of unintended migration.

We evaluated the effectiveness of BioAdheSil in securing three types of commercially available silicone stents: the Bonastent, Dynamic stent, and Dumon stent (**Figure 5b**). Before testing the tethering of the stents, we measured the bonding of fresh tracheal tissues to silicone substrates using lap-shear testing and found an adhesive strength ranging from 20-65 kPa (**Figure 5c**). To assess the adhesion of the silicone stents, each was implanted in *ex vivo* porcine tracheae of the matching size. BioAdheSil adhesive was then applied at the entire stent-trachea interface using a 5-Fr catheter. The efficacy of BioAdheSil in holding the stent in place was evaluated by measuring the anti-migration force, which was determined by displacing the stent by 20 mm and measuring the frictional force between the trachea and the stent (**Figure 5d**). On average, the anti-migration force was 3.5 times stronger for the Dumon stent, 4.5 times stronger for the Bonastent, and 3 times stronger for the Dynamic stent with BioAdheSil compared to without. (**Figure 5e**).

In cases where the airway anatomy is complex, standard stent sizes may not be suitable for a patient, and traditional airway stent manufacturing methods can be both costly and time-consuming, making customization difficult and may also be subject to regulatory constraints. We evaluate the effectiveness of using BioAdheSil adhesive as a solution for filling the gap at the interface and satisfying the required geometry.

To assess BioAdheSil's ability to conform to the geometric gaps, we conducted experiments using fresh tracheae of three different sizes: a tight fit, a relaxed fit, and a larger size that was a misfit. In all cases, the interfacial gap was filled with BioAdheSil to ensure complete coverage. The

implanted stents with and without BioAdheSil were then imaged using micro-computed tomography (μCT), and the reconstructed data is shown in **Figure 5f**. The interfacial gap area, highlighted in red, was quantified using ImageJ, and the results show negligible or no gaps at the interface when using BioAdheSil. BioAdheSil coating does not affect the material properties of commercial silicone stents, as demonstrated by compressive force measurement (flex force) during radial compression testing at up to 50% inner diameter displacement (Figures 5h and 5i). It should be noted that the mechanical properties of these stents differ significantly from those of the trachea. The purpose of measuring the compression force is to show that applying BioAdheSil to a standard-of-care device does not significantly change its material behavior.

This study provides new alternatives for addressing the challenge of size or shape mismatch during stent implantation, ultimately reducing the risk of migration by meeting the geometrical needs. The concept of BioAdheSil filling gaps between devices and tissues could be expanded to neuroprosthetics, where it can be used to securely anchor brain-computer interface electrodes to the delicate tissues of the brain or spinal cord using a soft and elastomeric material. This would ensure secure placement and prevent migration from the intended stimulation or recording site.[30]

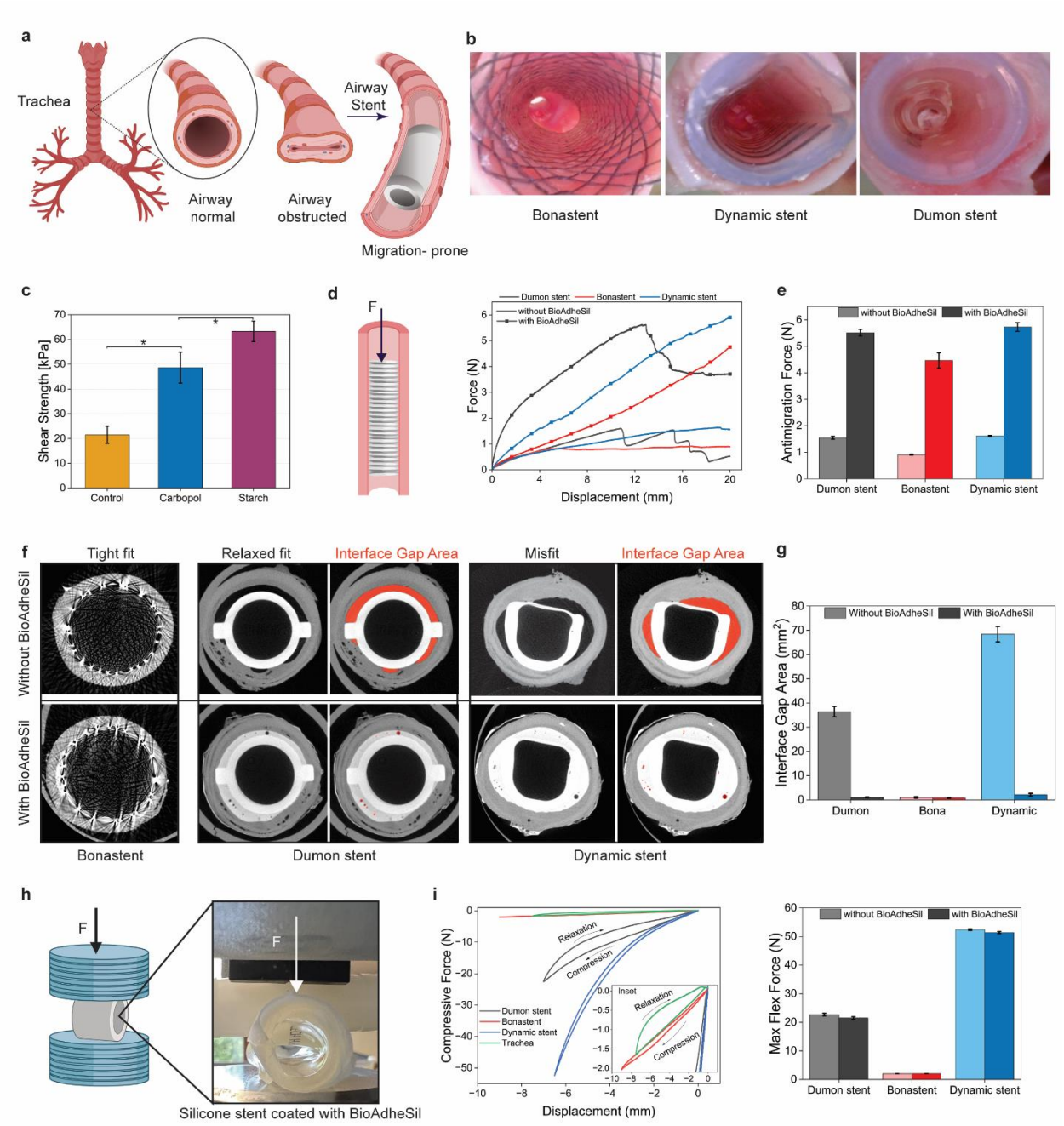

Figure 5: BioAdheSil for implantable silicone devices. (a) Silicone stents, which are used to alleviate airway obstruction or stenosis, are prone to migration due to an untethered interface and a mismatch between the device and anatomy. (b) Three commercially available silicone stents are employed to effectively adhere them to tracheal tissues using BioAdheSil. (c) The shear adhesion performance of BioAdheSil for adhering silicone sheets to tracheal tissues. Control, no water-absorbent additives. (d) Anti-migration force measurement. (e) Comparison of antimigration force for securing stents in tracheal tubes with or without BioAdheSil. (f) Filling of interfacial gap area between airway stent and tracheal anatomy using BioAdheSil, imaged under μCT (g) Quantified interfacial gap area before and after being filled with BioAdheSil. (h) Measurement set up for studying the effect of BioAdheSil coating on commercial airway stents. (i) Effect of

BioAdheSil coating on commercial stents, studied using a compression test. Values represent the mean and standard deviation (n=3), *p<0.05.

Providing an adhesive barrier to prevent bacterial infection at the exit site of transcutaneous devices

Left ventricular assist devices (LVADs) are mechanical pumps that are implanted in the chest to aid the heart in pumping blood. LVADs are increasingly being used for prolonging life in patients with advanced heart failure management, both as a bridge to transplant and destination therapy.[34] LVADs significantly enhance survival and quality of life for such patients. However, up to 40% of patients with LVADs face driveline infections.[35-37] The driveline, a thin tube connecting the LVAD pump to a power source and controller, exits percutaneously through an abdominal hole. These infections, marked by microbial colonization and inflammation around the driveline exit site, pose a serious concern in mechanical circulatory support (**Figure 6a**). They can result in various complications, including systemic infections, device malfunctions, and, in severe cases, sepsis and death. Effective management of driveline exit sites involves a meticulous driveline dressing regimen; and in the case of suspected or confirmed infection, antibiotic therapy, debridement, and relocation of the driveline in extreme cases.[38-39] Failure to take proper preventive measures to secure the driveline while engaging in excessive physical activity can cause trauma around the exit site, which can lead to neoepithelialization.[38-39] Neoepithelialization further impairs adherence and creates an environment favorable for microbial colonization. Therefore, the driveline must also be well-secured adjacent to the exit site to minimize movement.[35] Developing and applying a biofluid-resistant adhesive around the percutaneous exit site of LVAD drivelines would present a promising approach to preventing or controlling these infections.

To evaluate BioAdheSil as a treatment for securing the driveline, we designed a custom setup that simulates the skin-driveline junction. A skin incision was made using a skin biopsy punch to insert the driveline, and adhesive was applied to the central hole on the epidermal side to secure the LVAD driveline onto pig skin, as depicted in **Figure 6b**. The setup was secured to a mechanical tester, and the driveline was subjected to upward pulling with the pull-off force being recorded. BioAdheSil demonstrates a pull-off strength of 21 ± 2 N when the silicone portion of the driveline is bonded to porcine skin and 32 ± 4 N when the velour region (fabric layer) is bonded (**Figure 6c**). To compare the performance of BioAdheSil against existing commercial adhesives, we selected a diverse range of adhesives that represented different crosslinking chemistries and clinical indications, including stoma care, cardiac surgery, abdominal repair, and topical treatment. Among the adhesives tested, only Bioglue, Coseal, Dermabond, Liquiband, and BioAdheSil showed significantly stronger adhesion compared to the negative control (no adhesive used), as seen in **Figure**s **6d** and **6e**. To assess the water resistance of BioAdheSil and other commercial adhesives, we conducted a dye penetration test. A custom rig was 3D printed to secure the porcine skin, and a driveline was inserted through a central incision, which was then secured in place with various adhesives (Supplementary **Figure S11**). A dye was applied to the top of the epidermis, and any leaked dye was collected at the bottom and analyzed for light transmission through spectrophotometry. The level of transmitted light indicates the efficacy of the moisture barrier, serving as an indirect measure of preventing biofilm growth. Only BioAdheSil, Dermabond, and Liquiband were found to completely resist dye, a proxy for water and potentially microbial penetration (**Figure 6f**). Dermabond and Liquiband are based on

cyanoacrylate and are known to be stiff, and potentially damaging to the skin. Their use could result in further mechanical trauma at the exit site. In comparison, BioAdheSil offers 1.5 times stronger adhesion and comparable water resistance while being elastomeric, which allows for better strain release at the interface between the driveline and tissue. Our proposed strategy involves using non-starch BioAdheSil on the skin and starch-based BioAdheSil in the deep tissue tunnel up to a few millimeters below the dermal layer, as depicted in **Figure 6g**. The presence of starch in BioAdheSil will result in enzymatic degradation, leading to a porous material that may potentially promote the growth of fibroblasts and the formation of a stronger, infection-resistant collagen bond with the driveline through cell migration. *In vitro* incubation of BioAdheSil with the starch-degrading enzyme α-amylase creates a matrix with pores up to 245 ± 78 μm in size (**Figure 6h**, Supplementary **Figure S12**). These larger pores have been shown to facilitate deeper infiltration by macrophages, collagen, and blood vessels, i.e. driveline durable biointegration.[40-41] The formation of a porous matrix in 30% starch-based BioAdheSil is further supported by *in vivo* subcutaneous implantation in rats for a duration of 4 weeks, as evidenced by histological analysis (**Figure 6i**) and μCT imaging (**Figure 6j**). After a four-week of implantation, the non-starch-based BioAdheSil retains its film-like configuration without significant changes, whereas the 30% starch-based BioAdheSil exhibits signs of degradation, including a decrease in thickness and a fragmented configuration.

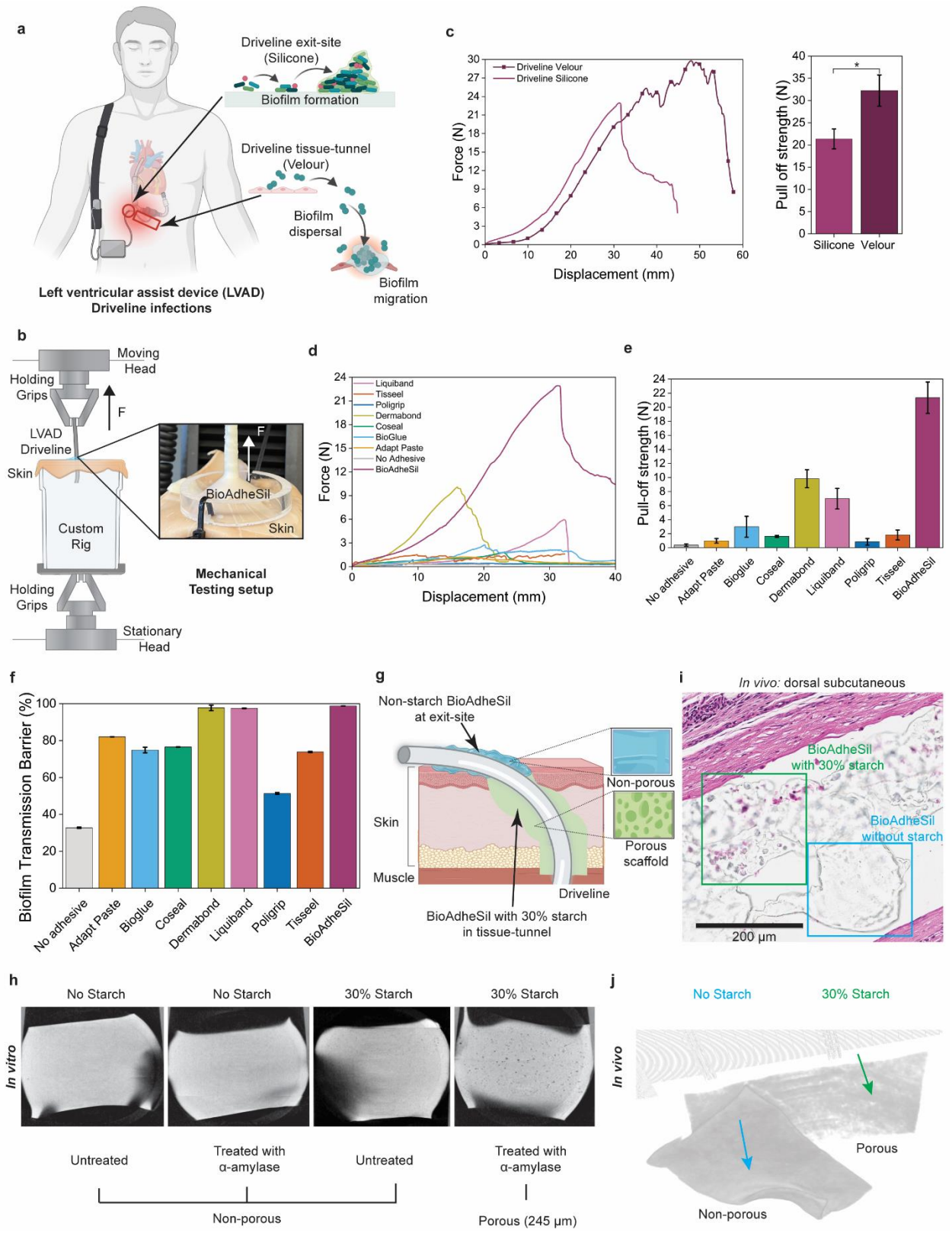

Figure 6: BioAdheSil for transcutaneous silicone devices. (a) An example of a transcutaneous implantation is the driveline for a Left Ventricular Assist Device (LVAD), which is inserted through the skin to connect the pump to the external controller and battery pack. This causes

biofilm migration due to a loose connection at the skin-driveline junction. (b) A custom-made test setup mimicking skin-driveline junction for evaluating adhesion strength. (c) Adhesion performance of BioAdheSil to bond different regions (silicone and velour) of driveline to porcine skin. (d) Force vs. displacement curves for adhering driveline with skin using BioAdheSil vs. a panel of commercial adhesives. (e) Comparison of pull-off strength between BioAdheSil and commercial adhesives. Control, no adhesive. (f) Comparison of biofilm transmission barrier between BioAdheSil and commercial adhesives. (g) Schematic illustrating the concept of using non-starch BioAdheSil as the top layer and 30% starch for adhesion to deeper tissues along the driveline tunnel. The degradation of starch increases the porosity of BioAdheSil, potentially facilitating cell integration. (h) An *in vitro* incubation process using α-amylase, a starch-degrading enzyme, on 30% starch BioAdheSil to create a porous matrix. Non-starch BioAdheSil is used as a control. The images were acquired using μCT. (i) Representative histological images of subcutaneously implanted 30% starch-based vs. non-starch-based BioAdheSil in the dorsal region, stained with hematoxylin and eosin (H&E), after a 4-week duration in a rat model. (j) Representative μCT images of 30% starch-based vs. non-starch-based BioAdheSil after a 4-week *in vivo* incubation in the dorsal subcutaneous region of a rat model. Values represent the mean and standard deviation (n=3-5), *$p<0.05$.

Based on our shear testing against the epidermis (see supplementary **Figures S13** to **S15** and Supplementary **Movie S1** for detailed epidermal skin-interfaced device adhesion characterization[42-52]) and subcutaneous tissue, assuming a 3 lb (heavier side) weight for the LVAD controller and battery pack, and a 2-foot external driveline extent (longer than usual to account for worst-case scenarios), if BioAdheSil is applied along the last 2 cm portion of the subcutaneous tract and around the exit side in the usual dressing distribution (similar to a 3M™ Tegaderm™ patch measuring 7 cm x 7 cm), the patient could potentially drop the controller and battery pack without experiencing delamination or adverse effects at the exit site, even without an anchor. Complete BioAdheSil application along the entire 1-foot internal tract would eliminate the need for dressing or an anchor altogether, potentially eliminating the logistical challenges of reapplication. This strategy studied for LVAD drivelines can also be easily adapted for use with peritoneal dialysis catheters or other tunneled lines, such as the peripherally inserted central catheter (PICC) lines and hemodialysis catheters.[53]

Conclusion

BioAdheSil, a silicone-based bioadhesive, is a new material that has been developed to improve the bonding of silicone medical devices to biological tissues. It uses a hydrophobic precursor to create a water-resistant bond, complemented by water-absorbing and biodegradable fillers that act as moisture buffers. This unique material design offers superior durability in adhering tissues and silicone devices while effectively resisting moisture and bodily fluids, which could otherwise deteriorate the adhesive bond over time. The water-absorbent fillers serve to prevent water ingress and absorb any penetrating moisture, ensuring the adhesive's structural integrity, and thereby preventing device displacement or detachment. The study explores the impact of different crosslinking agents and water-absorbent materials on the adhesion of silicone matrices to tissues. It demonstrates that BioAdheSil outperforms commercial adhesives in terms of adhesion strength, doesn't provoke an adverse host response during a 4-week implantation period, and promotes cell migration by transforming into a porous interface through enzyme degradation. In exemplary

applications, BioAdheSil proves its utility by addressing issues like size or shape mismatch in airway stent implantation. It ensures stronger adhesion between the stent and the inner tracheal lining, reducing the risk of migration. Additionally, BioAdheSil exhibits robust adhesion performance in securing LVAD drivelines in place and acts as a barrier against biofilm migration, thanks to its hydrophobic nature.

In summary, BioAdheSil stands as a versatile material with numerous possibilities for enhancing the adhesion of silicone medical devices to tissue, including implants and transcutaneous devices, offering improved device performance, usability and durability.

Methods

Adhesive Preparation

The SYLGARD™ 184 Silicone Elastomer Kit, comprising of silicone oligomers and siloxane coupling agents, was procured from Dow Corning. The fast-curing platinum-catalyzed silicone, Ecoflex™ 00-35 FAST, was acquired from Smooth-On Inc. Triethoxyvinylsilane (TEVS) and 3-(triethoxysilyl)propyl isocyanate (TEPI) silane crosslinkers were obtained from Sigma-Aldrich Inc. For the Sylgard polydimethylsiloxane elastomer, a 20:1 mixing ratio of silicone oligomers to siloxane coupling agents was employed. Meanwhile, equal parts of Part A and Part B were used for the Ecoflex silicone. TEPI and TEVS silane crosslinkers, each with a concentration range of 0.1 to 1.5 wt% of the total weight of precursor and coupling agents, were added to either the Sylgard PDMS siloxane coupling agent or to Ecoflex 00-35B. The silicone precursors were mixed with water absorbents or repellents, in varying weight percentages (3-60 wt%) of the total weight of the two parts of silicone. This included 3-60 wt% starch, purchased from Pure Supplements, USA, 3-30 wt% carbopol ETD 2020 from Lubrizol, and 3-30 wt% high-viscosity (100,000 cSt) silicone oil from Sigma-Aldrich Inc. The siloxane coupling agents with silane crosslinkers and the silicone precursors with water absorbents or repellents were combined just prior to application. Finally, a platinum(0)-1,3-divinyl-1,1,3,3-tetramethyl catalyst from Sigma-Aldrich Inc. was added to the PDMS matrix to regulate the curing time. This mixture was named BioAdheSil and was freshly prepared before each testing session. For bonding BioAdheSil to the intestinal lining, the TEPI crosslinker was substituted with 1.5 wt% of 3-aminopropyltriethoxysilane (APTES), which was acquired from Sigma-Aldrich Inc. Transglutaminase powder, procured from Modernist Pantry, was added to the final mixture to catalyze the bond formation between glutamine amino acids and amine groups.

Rheology

The gelation time and viscoelastic mechanical properties of each sample (n=3) were assessed using the AR 2000 parallel plate rheometer from TA-65 Instruments, under room temperature conditions. The measurements were carried out in real-time, utilizing a stainless-steel parallel plate probe with a diameter of 25 mm and a gap of 0.50 mm, applying a 1% strain and 1-Hz oscillation frequency.

Adhesion Characterization

The commercial adhesives used in this study were obtained from their respective manufacturers and the recommended curing and testing procedures were strictly followed. The collagen casings, used as tissue mimics for adhesion characterization to determine optimal amounts of silane

crosslinkers, water absorbents/repellents, and to compare cellulose vs. silicone adhesion, were acquired from The Sausage Maker. The fresh tissues were collected within two hours of animal sacrifice from the animal facility at the Massachusetts Institute of Technology (MIT), which is monitored by the Division of Comparative Medicine. The use and handling of *ex vivo* animal tissue in this study were approved by the Committee on Animal Care at MIT (with protocol number 0121-003-24). The fresh, thinly sliced porcine skin used for T-peel testing was procured from Sierra for Medical Science Inc., California. All mechanical testing was performed using the Instron 5944 mechanical tester equipped with a 100-N load cell. BioAdheSil was cured for 15 minutes and commercial adhesives were cured for the manufacturer's recommended time for all experiments. A sample size of n=3 was used for all types of specimens for adhesion testing unless specified otherwise.

Uniaxial testing

The mechanical tester was loaded with cured BioAdheSil adhesive sheets of dimensions 30 mm x 6 mm and a thickness of 2.5 mm. The sheets were uniaxially stretched at a rate of 100 mm/min until failure.

Lap-shear testing

For all experiments, tissue-mimicking collagen sheets, fresh porcine skin, and other biological specimens (such as trachea, intestinal wall, aortic wall, endocardium, myocardium, and pericardium) were cut to a standard size of 2.5 cm x 2.5 cm. The biological samples were secured onto microscopic glass slides using Loctite 422 instant adhesive. They were then sprayed with 1x phosphate-buffered saline (PBS) to mimic the moist tissue environment. Engineering materials, including silicone sheets and other materials like polyethylene terephthalate (PET), polyimide, thermoplastic polyurethane (TPU), cellulose, and Dacron polyester, were cut to a 2.5 cm x 2.5 cm size. The silicone sheets were attached to the glass slides using Sil-Poxy (Smooth-On) adhesive, while the other synthetic materials were bonded using Loctite 422 instant adhesive. A 0.3 mm thick adhesive layer was applied between the engineered materials and biological tissues with an overlap of 2.5 cm x 1 cm. The cured samples were then subjected to mechanical testing, following ASTM F2255-05 protocol, and pulled at a rate of 5 mm/min.

Peel testing

A 90-degree peel force was conducted following a modified ASTM D6862-11 protocol. A 25 mm x 25 mm hydrated collagen film was attached to microscopic glass slides using Loctite 422 instant adhesive. 75 mm x 25 mm strips of cellulose or silicone were then secured to the biological tissue using BioAdheSil or commercial adhesives. A 90° peel test was performed using a mechanical tensile tester, with the maximum peeling force recorded as the tester moved at a rate of 5 mm/min.

A T-peel adhesion test was carried out following ASTM F2256-05 protocol to determine peel force, adhesion energy, or interfacial toughness. Porcine skin strips, 2 mm thick and 75 mm x 20 mm in size, and similar-sized silicone strips were prepared. The samples were bonded using BioAdheSil along their entire length and then pulled at a tensile loading rate of 100 mm/min. Adhesion energy was calculated by multiplying the steady-state force by two and dividing the result by the 20 mm sample width. Both in the 90-degree and T-peel tests, a 0.08 mm thin PET

backing film was attached to the silicone strips using Loctite 422 to prevent stretching during tensile loading.

Tack testing

Biological tissue analogs (2.5 cm x 2.5 cm collagen sheets) and synthetic materials (cellulose) of the same size were attached to microscopic glass slides using Loctite 422 adhesive. Silicone substrates of the same size were attached to the glass slides using Sil-Poxy (Smooth-On) adhesive. An adhesive layer with a thickness of 300 μm (BioAdheSil and commercial adhesives) was placed between the wet collagen sheets and synthetic materials. The cured samples were subjected to tack strength testing using a mechanical tester with a tensile rate of 5 mm/min.

Attenuated Total Reflection Fourier-Transform Infrared spectroscopy (ATR FTIR)

The composition analysis of the tissue substrate (pig skin), cured BioAdheSil, and the assessment of the adhesion mechanism in real-time was carried out using Attenuated Total Reflection mode infrared spectroscopy. This data collection and analysis was performed using a Thermo Fisher FTIR6700 Fourier Transform Infrared Spectrometer. The data was acquired with a 4 cm^{-1} resolution with 64 scans, encompassing a scan range from 4,000 to 500 cm^{-1}.

Preparation of conductive composites

The conductivity of BioAdheSil adhesive was tuned by incorporating multi-walled carbon nanotubes (CNTs) in a range of 3-10% weight percentage. The CNTs were sourced as a powder from Cheap Tubes Inc. The electrical resistance was measured using a two-point probe setup and a Keithley 2450 Sourcemeter set to 1 V. The resulting current was used to calculate the resistance using Ohm's law. Thin strips, 20 mm x 10 mm in size and 3 mm in thickness were prepared for each weight percentage of CNTs and tested for resistance.

X-ray micro-computerized tomography (μCT)

A micro-computerized tomography (μCT) using a Skyscan 1276 X-ray microtomograph from Bruker was conducted to assess BioAdheSil-interfaced medical wearables and tracheal stents, as well as to analyze the porosity of enzymatically degraded BioAdheSil *in vitro* and *ex vivo* after 4-week subcutaneous implantation. Aluminum and copper filtering were used during imaging, with an acquisition time of 6 minutes per sample. The data was processed using NRecon software, viewed with Dataviewer, and visualized in 3D with CTVOX from Bruker.

Adhesion to ZIO® XT cardiac patch and interface evaluation

The adhesion of the ZIO® XT cardiac patch monitor by iRhythm Technologies was evaluated using a T-peel force measurement test (loading rate 5 mm/min) with BioAdheSil adhesive on wet porcine skin. The performance of BioAdheSil was compared to the commercial skin adhesives (the adhesive provided with the ZIO® XT cardiac patch and a cyanoacrylate-based Dermabond adhesive). After delamination, the interface was examined using μCT, and the images were color-coded for easy identification of the adhesive, device, and tissue. The adhesive is gray, the skin is beige, and the device is blue in color.

Antimigration force characterization

The efficacy of BioAdheSil was tested by adhering commercially available tracheal stents to tracheal tissue. The stents used were the Boston Scientific Dynamic Y Stent (13mm x 10mm), the Bonastent Tracheal/Bronchial (18mm x 50mm), and the Boston Medical Dumon TD Silicone Tracheal-Broncheal Stent (14mm x 50mm). The tracheal stents were bonded to freshly harvested tracheal tubes by delivering the adhesive at the interface through a single lumen, 5 Fr umbilical venous catheter (Cardinal Health) and later tested for migration by moving them a distance of 20 mm at a rate of 5 mm/min using a mechanical tester. The antimigration force, or the frictional force between the stent and the airway, was recorded for all cases, including a control where no adhesive was used.

Flex force characterization

To determine the impact of BioAdheSil on the mechanical properties of the stents, the flexibility of BioAdheSil-coated stents was measured in response to 50% compression of their inner diameter at a rate of 100 mm/min. The compressive force was recorded as the flex force.

LVAD driveline pull-off force

The HeartMate 3™ Left Ventricular Assist Device (LVAD) driveline by Abbott Cardiovascular was used to test the adhesion strength of BioAdheSil on porcine skin. Fresh and thick porcine skin with a layer of muscle and fascia was used. A 6 mm incision was made in the center of the skin using a skin coring biopsy punch, and the driveline was inserted through the hole and secured with BioAdheSil and several commercially available adhesives. After curing, the adhesive-interfaced skin and driveline assembly was mounted to a mechanical tester with a custom rig. The driveline was then pulled upward at a rate of 100 mm/min until failure, and the pull-off force was recorded.

Transmission barrier testing

A dye penetration test was conducted to assess the moisture barrier properties of the BioAdheSil-interfaced skin and driveline assembly. A custom-made rig was created by 3D printing to support the recently harvested pig skin, and a driveline was inserted through a central incision measuring 6 mm in diameter. The driveline was then fixed in place using various adhesives by applying a 500-700 µm thick layer. 5 ml of undiluted gentian violet dye was applied to the top of the epidermis and allowed to sit for 15 minutes. Any leaked dye was collected at the bottom after 15 minutes, and the bottom side of the skin/driveline interface was washed with 5 ml of distilled water. The amount of light transmitted through the eluted dye was analyzed using spectrophotometry after the dye was transferred to a cuvette.

***In vitro* starch degradation**

The degradation of BioAdheSil films infused with starch was evaluated *in vitro* by incubating them with an α-amylase solution. 30 wt% starch-infused and non-starch BioAdheSil films were subjected to a two-week incubation process with a 50 w/v% of alpha-amylase from the porcine pancreas in 1x PBS. α-Amylase was purchased from Sigma-Aldrich Inc. After incubation, the films were washed three times with 1x PBS, and their porosity was evaluated using µCT imaging. The pore size was quantified through image processing using ImageJ, as seen in the supplementary **Figure S5**.

***In vivo* subcutaneous implantation in rats**

All animal procedures were thoroughly reviewed and approved by the Massachusetts Institute of Technology Committee on Animal Care (approval number #0121-003-24) in accordance with the guidelines set forth by the National Research Council's Guide for the Care and Use of Laboratory Animals. Prior to implantation, rectangular 30% starch-based and non-starch-based BioAdheSil samples measuring 10 mm x 5 mm were prepared using sterile techniques and further sterilized through the Ethylene Oxide (EtO) sterilization process.

For the implantation procedure, two Sprague Dawley rats weighing 275 g and 340 g were anesthetized using isoflurane (1–3% isoflurane in oxygen) in an anesthetizing chamber. The dorsal region was prepared by removing the hair, and the rats were placed on a heating pad throughout the surgery. Anesthesia was continuously administered through a nose cone. After the application of eye ointment and administration of 2cc of saline, access to the subcutaneous space was achieved by making a 1 cm incision per implant. In each rat, a rectangular 30% starch-based sample (n = 4) and a non-starch-based BioAdheSil sample (n = 4) were inserted into the subcutaneous pockets created underneath each of the four incisions. The incisions were closed using biodegradable interrupted sutures (4-0, Ethicon) and skin glue (VetBond).

After a 4-week period following the implantation, the animals were euthanized using CO_2 inhalation. The subcutaneous regions of interest were excised and fixed in 10% formalin for 24 hours to facilitate histological and immunohistochemistry analyses.

Statistical Analysis

Data were collected from a minimum of three repetitions and analyzed for the mean and standard deviation, unless otherwise specified. The results were analyzed and plotted using OriginPro 2021b (64-bit). The statistical significance ($*p < 0.05$) was evaluated through a one-way ANOVA analysis with Tukey correction in OriginPro 2021b.

Data Availability Statement

All original data presented in the study are documented in the main article and supplementary material. For further inquiries, please contact the corresponding author.

Conflict of Interest

E.T.R. serves on the board of directors for Affluent Medical and Helios Cardio, and also serves on the board of advisors for Pumpinheart. In addition, E.T.R. provides consulting services for Holistick Medical and is a co-founder of Fada Medical and Spheric Bio. D.L.T. serves on the board of directors for SurgiBox Inc. M.R.M. reports receiving payments from Abbott for consulting services. M.R.M. also discloses receiving consulting fees from Mesoblast, Janssen, Moderna, Paragonix, and Baim Institute for Clinical Research. Furthermore, M.R.M. is an advisory board member for Transmedics, NuPulseCV, Leviticus, and FineHeart. All other authors declare no conflict of interest.

Funding

This research was funded by the National Science Foundation (grant number 1847541, awarded to E.T.R.) and the William Harvey Distinguished Chair in Advanced Cardiovascular Medicine fund (awarded to M.R.M). S.X.W. acknowledges funding from the National Institutes of Health training grant T32 HL007734.

Acknowledgments

The authors express gratitude to the Animal Imaging and Pre-Clinical Testing Core Facility at the Massachusetts Institute of Technology (MIT) for allowing to use the X-ray μCT. They also acknowledge the MIT Institute for Soldier Nanotechnologies for the use of their Rheometer. The figures and digital illustrations were created using Adobe Illustrator, Adobe Photoshop, ChemDraw Professional, and BioRender.com. The photo used in the supplementary Figure S13a was obtained from unsplash.com under the Unsplash License. The data were plotted and analyzed using OriginPro 2021b software.

Supplementary Material

The supplementary material for this article can be accessed online at:

References

Uncategorized References

[1] L. W. McKeen, in *Handbook of polymer applications in medicine and medical devices*, Elsevier, **2014**, pp. 21-53.
[2] B. P. Staff*, Vol. AVM207A*, **2021**.
[3] S. Rajaram*, Vol. CHM100A*, **2020**.
[4] PC32-85, **2022**.
[5] PD3F-85, **2022**.
[6] P. Lee, E. Kupeli, A. C. Mehta, *Interventional Pulmonary Medicine* **2016**, 61-76.
[7] J. Turner, W. Shain, D. Szarowski, M. Andersen, S. Martins, M. Isaacson, H. Craighead, *Experimental neurology* **1999**, *156*, 33-49.
[8] M. Singh, H. S. Nanda, R. D. O'Rorke, A. E. Jakus, A. H. Shah, R. N. Shah, R. D. Webster, T. W. Steele, *Advanced healthcare materials* **2018**, *7*, 1800538.
[9] Y.-T. Kim, R. W. Hitchcock, M. J. Bridge, P. A. Tresco, *Biomaterials* **2004**, *25*, 2229-2237.
[10] J. Cyrany, S. Rejchrt, M. Kopacova, J. Bures, *World J Gastroenterol* **2016**, *22*, 618-627.
[11] N. V. Pavlovic, T. Randell, T. Madeira, S. Hsu, R. Zinoviev, M. Abshire, *Heart & Lung* **2019**, *48*, 90-104.
[12] P. C. Morss-Walton, J. Z. Yi, M. E. Gunning, J. S. McGee, *Dermatologic Therapy* **2021**, *34*, e15069.
[13] C. Park, Y. Fan, G. Hager, H. Yuk, M. Singh, A. Rojas, A. Hameed, M. Saeed, N. V. Vasilyev, T. W. J. Steele, X. Zhao, C. T. Nguyen, E. T. Roche, *Science Robotics* **2020**, *5*, eaay9106.
[14] H. Saraf, K. Ramesh, A. Lennon, A. Merkle, J. Roberts, *Journal of biomechanics* **2007**, *40*, 1960-1967.
[15] G. Singh, A. Chanda, *Biomedical Materials* **2021**, *16*, 062004.
[16] C. Cui, T. Wu, X. Chen, Y. Liu, Y. Li, Z. Xu, C. Fan, W. Liu, *Advanced Functional Materials* **2020**, *30*, 2005689.
[17] H. Fan, J. Wang, J. P. Gong, *Advanced Functional Materials* **2021**, *31*, 2009334.
[18] H. Yuk, C. E. Varela, C. S. Nabzdyk, X. Mao, R. F. Padera, E. T. Roche, X. Zhao, *Nature* **2019**, *575*, 169-174.
[19] S. J. Wu, H. Yuk, J. Wu, C. S. Nabzdyk, X. Zhao, *Advanced Materials* **2021**, *33*, 2007667.
[20] Y. Hou, Y. Li, Y. Li, D. Li, T. Guo, X. Deng, H. Zhang, C. Xie, X. Lu, *ACS nano* **2023**, *17*, 2745-2760.
[21] J. Li, A. Celiz, J. Yang, Q. Yang, I. Wamala, W. Whyte, B. Seo, N. Vasilyev, J. Vlassak, Z. Suo, *Science* **2017**, *357*, 378-381.
[22] N. R. Wolf, X. Yuan, H. Hassani, F. Milos, D. Mayer, U. Breuer, A. Offenhäusser, R. Wördenweber, *ACS Applied Bio Materials* **2020**, *3*, 7113-7121.
[23] Q. Liu, G. Nian, C. Yang, S. Qu, Z. Suo, *Nature communications* **2018**, *9*, 846.

[24] J. M. Orban, L. B. Wilson, J. A. Kofroth, M. S. El-Kurdi, T. M. Maul, D. A. Vorp, *Journal of biomedical materials research Part A* **2004**, *68*, 756-762.

[25] M. Singh, I. Solic, T. W. Steele, *ACS Macro Letters* **2021**, *10*, 1353-1358.

[26] A. E. Jakus, E. B. Secor, A. L. Rutz, S. W. Jordan, M. C. Hersam, R. N. Shah, *ACS nano* **2015**, *9*, 4636-4648.

[27] M. A. Bhat, R. A. Rather, A. H. Shalla, *Synthetic Metals* **2021**, *273*, 116709.

[28] Y. S. Negi, P. Adhyapak, *Journal of Macromolecular Science, Part C: Polymer Reviews* **2002**, *42*, 35-53.

[29] M. Zhang, Z. Tang, X. Liu, J. Van der Spiegel, *Nature Electronics* **2020**, *3*, 191-200.

[30] X. Tang, H. Shen, S. Zhao, N. Li, J. Liu, *Nature Electronics* **2023**.

[31] L. Freitag, A. Ernst, M. Unger, K. Kovitz, C. Marquette, *European Respiratory Journal* **2007**, *30*, 7-12.

[32] E. Folch, C. Keyes, *Annals of cardiothoracic surgery* **2018**, *7*, 273.

[33] N. Paunović, Y. Bao, F. B. Coulter, K. Masania, A. K. Geks, K. Klein, A. Rafsanjani, J. Cadalbert, P. W. Kronen, N. Kleger, *Science Advances* **2021**, *7*, eabe9499.

[34] J. L. Vieira, H. O. Ventura, M. R. Mehra, *Progress in Cardiovascular Diseases* **2020**, *63*, 630-639.

[35] L. T. Yarboro, J. D. Bergin, J. L. Kennedy, C. C. Ballew, E. M. Benton, G. Ailawadi, J. A. Kern, *Annals of cardiothoracic surgery* **2014**, *3*, 557.

[36] S. Roest, H. I. Bax, N. J. Verkaik, J. J. Brugts, A. A. Constantinescu, C. C. de Bakker, O. Birim, K. Caliskan, O. C. Manintveld, *International Journal of Infectious Diseases* **2020**, *92*, 127-129.

[37] C. B. Patel, L. Blue, B. Cagliostro, S. H. Bailey, J. W. Entwistle, R. John, V. Thohan, J. C. Cleveland Jr, D. J. Goldstein, N. Uriel, *The Journal of Heart and Lung Transplantation* **2020**, *39*, 774-781.

[38] D. Pereda, J. V. Conte, *Cardiology clinics* **2011**, *29*, 515-527.

[39] O. Saeed, N. Moss, B. Barrus, H. Vidula, S. Shah, S. Feitell, K. S. Masser, A. Kilic, D. Moin, P. Atluri, *Artificial Organs* **2022**, *46*, 1409-1414.

[40] F. J. O'Brien, B. Harley, I. V. Yannas, L. J. Gibson, *Biomaterials* **2005**, *26*, 433-441.

[41] S. Kalaba, E. Gerhard, J. S. Winder, E. M. Pauli, R. S. Haluck, J. Yang, *Bioactive Materials* **2016**, *1*, 2-17.

[42] S. M. Iqbal, I. Mahgoub, E. Du, M. A. Leavitt, W. Asghar, *NPJ Flexible Electronics* **2021**, *5*, 9.

[43] FDA, in *Product Code: DSH; Product Problem: Loss of or Failure to Bond, Vol. Product Code: DSH; Product Problem: Loss of or Failure to Bond*, The United States Food and Drug Administration, https://www.accessdata.fda.gov/, **2018-2019**, p. Periodical: Product Code: DSH; Product Problem: Loss of or Failure to Bond.

[44] FDA, The United States Food and Drug Administration, https://www.accessdata.fda.gov/CDRH510K/K143513.pdf, **2014**.

[45] M. A. Rosenberg, M. Samuel, A. Thosani, P. J. Zimetbaum, *Pacing and Clinical Electrophysiology* **2013**, *36*, 328-333.

[46] L. McNichol, C. Lund, T. Rosen, M. Gray, *Orthopaedic Nursing* **2013**, *32*, 267-281.

[47] G. Stamatas, J. Nikolovski, M. Mack, N. Kollias, *International journal of cosmetic science* **2011**, *33*, 17-24.

[48] T. Clarke, *Journal of Plastic, Reconstructive & Aesthetic Surgery* **2011**, *64*, e170-e173.

[49] K. Cutting, *Journal of Wound Care* **2008**, *17*, 157-162.

[50] M. L. Shannon, C. A. Lehman, *Critical care nursing clinics of North America* **1996**, *8*, 17-28.

[51] M. A. Smith, N. M. Jones, S. L. Page, M. P. Dirda, *Journal of the American Institute for Conservation* **1984**, *23*, 101-113.

[52] A. Rosenberg, R. Williams, G. Cohen, *Journal of pharmaceutical sciences* **1973**, *62*, 920-922.

[53] A. Peppelenbosch, W. H. Van Kuijk, N. D. Bouvy, F. M. Van der Sande, J. H. Tordoir, *NDT plus* **2008**, *1*, iv23-iv28.

The table of contents (ToC)

This study presents a silicone-based bioadhesive designed to create strong bonds between silicone devices and biological tissues. It combines wet tissue adhesion with long-term integration capabilities, transitioning from non-permeable to permeable over time to facilitate cell migration. Experimental results demonstrate superior performance compared to commercial adhesives, with no adverse reactions observed in rats. This holds promise for diverse applications, including implantable and transcutaneous medical device adhesion.